



The threshold of amyloid aggregation of beta-lactoglobulin: Relevant factor combinations

Timon R. Heyn^a, Julian Mayer^b, Hendrikje R. Neumann^c, Christine Selhuber-Unkel^c, Arno Kwade^b, Karin Schwarz^a, Julia K. Keppler^{a,d,*}

^a Institute of Human Nutrition and Food Science, Division of Food Technology, Kiel University, 24118, Kiel, Germany

^b Institute of Particle Technology, Technical University Braunschweig, 38106, Braunschweig, Germany

^c Institute of Materials Science, Department for Biocompatible Nanomaterials, Kiel University, 24143, Kiel, Germany

^d Laboratory of Food Process Engineering, Wageningen University, 6708 PB, Wageningen, the Netherlands

ARTICLE INFO

Keywords:

Whey protein
Beta-lactoglobulin
Amyloid aggregates
Fibrils
Statistical experimental design
Factor combinations

ABSTRACT

This study identifies critical factor combinations of pH, temperature, stirring speed, protein and ion concentration that specifically affect the lag-, and growth phase of beta-lactoglobulin amyloid aggregation and provides information on how, when and why certain factor combinations affect the onset of amyloid aggregation.

Conditions at the threshold of amyloid formation were chosen to prolong the lag and growth phase for several hours. Temperature was the most important factor in all aggregation stages. Interactions between low pH and temperature in the growth phase were caused by elevated protein denaturation at low pH (DSC). Interactions between stirring speed and temperature in the lag phase were caused by viscosity-dependent shear stress (CFD-simulation).

Even if none of the factor combinations could shift the onset of amyloid aggregation, important factor combinations were identified that favour the onset of amyloid aggregation. Therefore, the results of this study could be relevant for industrial production.

1. Introduction

One of the most frequently studied fibril forming proteins in whey is beta-lactoglobulin (BLG), which forms several micrometre long fibres at low pH values and high temperatures after several hours of incubation (Jung et al., 2008; Loveday et al., 2010; Nicolai and Durand, 2013). BLG-fibrils are of industrial interest because of their improved functional properties to form gels (Mohammadian and Madadlou, 2016), stabilise foams (Peng et al., 2017) and emulsions (Gao et al., 2017), as well as for microencapsulation (Serfert et al., 2014). Additionally, their potential for nano- and biomaterial applications are of increasing interest (Knowles and Mezzenga, 2016).

In order to use the entire functional potential of the aggregates, the formation of temperature-induced BLG fibrils should be investigated in detail. In recent years, this has led to the intensive study of various influencing factors.

The pH value is the primary influencing factor for acid hydrolysis, providing peptide building blocks for the semiflexible fibrils at pH

values < 3.0 (Akkermans et al., 2008b; Ye et al., 2018), while unhydrolysed proteins aggregate at pH values ≥ 3.5 (Keppler et al., 2019). Simultaneously, pH-related electrostatic repulsion affects the ordered aggregation—and thus the different fibril morphologies—observed with increasing pH value (Loveday et al., 2010).

Since incubation temperature significantly affects protein denaturation and acid hydrolysis, it is a key factor for the aggregation kinetics (Loveday et al., 2012b; Loveday, 2016). Also the molecular motion (Ciucu et al., 2016; Dvorsky et al., 2000; Einstein, 1905) and dielectric constant (Havinga, 1961; Pitera et al., 2001; Zhu et al., 2015) of the protein solution are influenced by the incubation temperature. Both factors in turn influence protein interactions.

Likewise, protein concentration is related to interaction effects between particles in the solution (Arnaudov and Vries, 2006) and thus influences the aggregation kinetics (Pellarin and Caflich, 2006) and morphology (Ye et al., 2018).

Moreover, the ion concentration reduces the charge of the particles and thus the electrostatic repulsion effects (Loveday et al., 2017) which results in different morphologies and aggregation kinetics (Loveday

* Corresponding author. Laboratory of Food Process Engineering, P.O. Box 17, 6700 AA, Wageningen, the Netherlands.

E-mail addresses: theyn@foodtech.uni-kiel.de (T.R. Heyn), j.mayer@tu-braunschweig.de (J. Mayer), hn@tf.uni-kiel.de (H.R. Neumann), cse@tf.uni-kiel.de (C. Selhuber-Unkel), a.kwade@tu-bs.de (A. Kwade), info@foodtech.uni-kiel.de (K. Schwarz), julia.keppler@wur.nl (J.K. Keppler).

<https://doi.org/10.1016/j.jfoodeng.2020.110005>

Received 21 November 2019; Received in revised form 27 February 2020; Accepted 2 March 2020

Available online 4 March 2020

0260-8774/© 2020 The Authors. Published by Elsevier Ltd. This is an open access article under the CC BY license (<http://creativecommons.org/licenses/by/4.0/>).

Abbreviations

BLG	Beta-Lactoglobulin
ThT	Thioflavin-T
AFM	Atomic Force Microscopy
ATR-FTIR	Attenuated Total Reflection Fourier Transform Infrared Spectroscopy
DSC	Differential Scanning Calorimetry
CFD	Computational Fluid Dynamics
VOF	Volume of Fluid
DOE	Design of Experiments

et al., 2010).

Stirring speed provides additional energy to the protein solution and leads to a turbulent shear flow, which influences the particle motion with respect to particle collision while exerting a certain level of shear stress on the protein (Bliatsiou et al., 2018; Ng et al., 2016). Therefore, moderate stirring enhances the amyloid aggregation (Bolder et al., 2007; Ng et al., 2016) by shortening the lag phase (Dunstan et al., 2009).

Notably, the incubation time can be viewed as an amplifier of the previous factors. Amyloid aggregation can be divided into the time-dependent lag, growth and termination phase (Loveday et al., 2017). The lag phase is characterised by providing the fibril building blocks and can be skipped or shortened by adding so-called “seeds” (Loveday et al., 2012a). Fibril growth begins with nucleation, whereby the proteins/peptides are first reversibly and then tightly bound together (Pellarin and Cafisch, 2006). The termination phase is purported to be caused by the depletion of available building blocks (Loveday et al., 2017).

However, to date the influence of factor combination on the lag and growth phases were only investigated under optimal conditions (temperature >80 °C, pH value < 2.5) for fibril formation (Loveday et al., 2011). It can be hypothesised that a combination of the necessary factors (discovered by screening) with other optional factors might also affect fibril formation and that during the lag phase other factor combinations than in the growth or stationary phase are relevant. In addition to identifying these factor combinations, the present study also aims to elucidate their underlying mechanisms in further experiments.

The investigation of this critical point provides information on how strongly, when and why certain factor combinations are capable of shifting the threshold of amyloid aggregation. Since a major challenge is the detection of minimal fibrillation, several independent methods were used, including mechanical separation (ultrafiltration), structure characterisation (Fourier transform infrared spectroscopy (FTIR)), fluorescence spectroscopy (Thioflavin-T (ThT)-assay), and the imaging of aggregates (atomic force microscopy (AFM)). To obtain a mechanistic understanding of the factor combinations, additional experiments were conducted with differential scanning calorimetry (DSC) and computational fluid dynamics (CFD) modelling.

2. Materials and methods

2.1. Materials

BLG was obtained from *Davisco Foods International Inc.* (Eden Prairie, US) with 97% protein and 96% BLG in dry matter. Calculated NaCl content was 49.6 $\mu\text{mol g}^{-1}$ protein. ThT (>95%) acid was obtained from *EMD Chemicals Inc.*, while all additional chemicals were obtained from *Sigma Aldrich Inc* were analytical grade. All experiments were conducted with ultra-pure water (>17 M Ω ; total oxidizable carbon <5 ppb).

2.2. Methods

2.2.1. Preparation of BLG solutions and production of BLG fibrils

For screening BLG fibril solutions were prepared as described by Heyn et al. (2019).

To screen the effects of protein concentration, pH value, temperature, stirring velocity and NaCl concentration, only one of these parameters was changed at a time (Table 1). The pH values of the solutions were adjusted with 6 M HCl and experiments were conducted in 100 ml Schott bottles with a 8.5 \times 2 mm cylindrical stirring bar.

For the design of experiments (DOE) the parameters used are provided in Table 2. Water bath temperature was controlled and protocolled using an EBI 2 temperature logger (*Ebro Elektronik GmbH*, Germany).

After 0.5, 1, 2, 3, 4 and 5 h, samples were taken and cooled in an ice-water bath for 30 min and stored at 4 °C until further use. For all following dilution processes, pH-adjusted Milli-Q-Water was used.

2.2.2. Physicochemical characterization of native and fibrillar BLG

To monitor fibril growth during incubation, the development of amyloid beta sheets was followed by the intensity of Thioflavin-T-fluorescence (ThT FL) and the conversion rate was analysed by centrifugal ultrafiltration. The secondary structure was analysed using ATR-FTIR and fibril morphology by AFM. The concentrations of monomer and peptide material were analysed via size exclusion chromatography (SEC) from dissociated samples and the level of hydrolysis was calculated from the loss of monomeric BLG. All these experiments were performed following the protocol of Heyn et al. (2019).

To obtain numerical values for the relative changes in beta-sheets, respective changes in the intensities of the second derivative of FTIR wavenumber 1632 cm^{-1} (intramolecular beta-sheets) and FTIR band wavenumber 1622 cm^{-1} (intermolecular beta-sheets) were determined. From the numerical intensity values at the respective wavenumbers at time t_i , the intensity values of the same wavenumber at time t_0 of the respective measurement series were subtracted. Mean and standard deviation were calculated from triplicate measurements.

2.2.3. Differential scanning calorimetry (DSC)

DSC was performed using the DSC250 (*TA Instruments*, New Castle, USA). BLG solution with 1 wt% was prepared as described by Heyn et al. (2019) and adjusted to the respective pH values of 2.0, 2.5 and 3.0.

The temperature was increased by 5 °C min^{-1} to a final temperature of 110 °C, followed by an isothermal phase for 1 min. The temperature was then decreased by 20 °C min^{-1} to a final temperature of 20 °C, followed by an isothermal phase of 1 min. Temperature-ramps to 110 °C and 20 °C were then repeated without isothermal phases. The enthalpy, as well as the onset and peak of denaturation temperature, were then calculated.

2.2.4. Statistical analysis of screening, DOE and fitting of values

Statistical analysis of the collected data was conducted by GraphPad PRISM (*version 6.07*, *GraphPad Software*, San Diego, USA). A significant increase of the ThT-values was verified by two-way ANOVA with Tukey's multiple comparison test at the 0.05- significance level. The

Table 1
Parameters used for the screening.

Parameters	Basic parameters	Additional parameters
Temperature [°C]	90	40, 55, 70, 75, 85, 95
pH value	2	1*, 3, 4, 5, 6, 7, 8, 9, 10*, 11*, 12*
Protein concentration [wt %]	2.5	0.1, 0.25, 0.5, 1, 1.5, 5
NaCl concentration [mM]	0	5, 15
Stirring velocity [RPM]	350	0, 700, 1300

*no data available for Fourier transform infrared spectroscopy.

Table 2
Parameters used for the design of experiments.

Parameters	Level-1-factors	Center-point-factors	Level-2-factors
Temperature [°C]	70	72.5	75
pH value	2.5	2.75	3
Protein concentration [wt %]	1	1.25	1.5
NaCl concentration [mM]	0	5	10
Stirring velocity [RPM]	200	250	300

increase of ThT-values as a function of time was fitted by the sigmoidal equation

$$f_t = \alpha + ((\beta - \alpha)/(1 + \exp((\gamma - t)/k)))$$

in where f_t is fluorescence at time t , k is the slope and α , β and γ are arbitrary constants.

Level of hydrolysis was fitted by an exponential plateau equation

$$h_t = h_0 - (h_0 - h_m) \exp(-k \cdot t)$$

in where h_t is the level of hydrolysis at time t , k is the rate constant, h_0 is the amount of hydrolysed material at t_0 and h_m is the maximum amount of hydrolysed material.

For the DOE, the means of the responses “ThT-intensity” and “fibril yield” were calculated. The DOE was planned and evaluated by Stat-Ease Design-Expert (version 10.0.7.0 Stat-Ease Inc., Minneapolis, USA). A fractional 2level 5factorial design type with three centre points and one replicate was created.

2.2.5. Computational fluid dynamics (CFD)

CFD were used to obtain additional information regarding the influence of flow and stress parameters during amyloid fibril formation of BLG. The exact shape of the Schott bottle was provided by the manufacturer and the dimensions of the stirring bar were measured manually. The geometries used in the simulation were created using SolidEdge ST9 in stereolithography (STL) format. The simulations were conducted with open-source software OpenFOAM-5.0. The solver interDyMFoam was chosen for isothermal non-miscible incompressible fluids and multi-phase flow with the volume of fluid (VOF) method, which includes mesh motions, optional topology changes and adaptive re-meshing. The mesh generation was performed with the tools “blockMesh” for the basic mesh (60 cells in x, y, and z direction each) and “snappyHexMesh” for the implementation of the STL geometries as well as the detailing and refinement of the mesh. The refined mesh has a total cell number of 299,212. A section through the created mesh can be seen in Fig. 1 (a). A finer mesh was created in the area of the glass walls and the stirring bar to account for zones of high velocities and stressing. As evident in Fig. 1

(b), a rotational zone with the OpenFOAM method of arbitrary mesh interfaces (AMI) was generated to perform the rotation of the stirring bar. The stirring bar velocity was set to 20.944 (200 RPM) and 31.416 rad s⁻¹ (300 RPM), respectively. The regions of suspension and air were generated with “setFields” in such a way that the glass was filled with suspension up to a height of 19 mm. The standard k-ε model was used to deal with turbulent flow in the stirred fluid. The basic governing equations (conservation of mass and momentum) were calculated using the basic Navier-Stokes and Reynolds-Averaged equations. The equations of continuity and motion were solved to attain velocities and velocity profiles, eddy energy (k) and eddy dissipation (ε). Thereafter, shear rates and shear stresses were calculated, with images of the setup and flow pattern being generated using ParaView 5.4.0. For the initial conditions at the walls, a zero flux was imposed to computational domains and gravity was set to 9.81 m s⁻² in the negative vertical direction. The viscosity of the fluid was modelled as Newtonian in the relevant shear rate range above 1 s⁻¹. The viscosity parameters were determined by a shear rate ramp (10⁻⁴ to 10³ s⁻¹) at 70 °C and 75 °C of 1.25 wt% BLG and fibril solutions with a Bohlin Gemini rheometer (Rotometric drive 2, Malvern Instruments, Malvern, UK) equipped with double gap geometry.

The shear-thinning behaviour of the fibrils and the specific viscosities, which are passed through between the start and end time, were not taken into account. The surface tension of the suspension was set to the constant 72.75E-03 kg s⁻².

3. Results & discussion

3.1. Screening for the threshold of amyloid aggregation

The influence of acidic pH values (i.e., pH 1–4), temperature (i.e., 55–95 °C), protein concentration (0.1–5 wt%), stirring speed (0–1300 RPM) and ion concentration (0–15 mM NaCl) on fibril formation were screened during a period of 5 h using the ThT-assay and FTIR. The influence of the pH value on morphology was also investigated by AFM.

The observed threshold parameters were observed to be in a temperature range between 70 and 75 °C (Fig. 2 C and D) since no significant aggregation was observed below 70 °C during 5 h incubation at pH 2. At 90 °C, the threshold pH value range was between pH 2.5 to 3 (Fig. 2 A and B) since evidence for the first occurrence of wormlike aggregates together with fibrils was observed at pH 3. This indicates an altered amyloid-like morphology and aggregation behaviour from straight fibrils to worm-like aggregates (Keppler et al., 2019), while only straight fibrils were evident in representative AFM images at pH 2 (Heyn et al., 2019). While higher protein concentrations resulted in higher ThT FL intensities (Fig. 2 E and F), the proportion of intermolecular beta-sheets did not differ significantly. Therefore, a range between 1 and 1.5 wt% protein concentration was chosen at pH 2 and 90 °C. Low protein

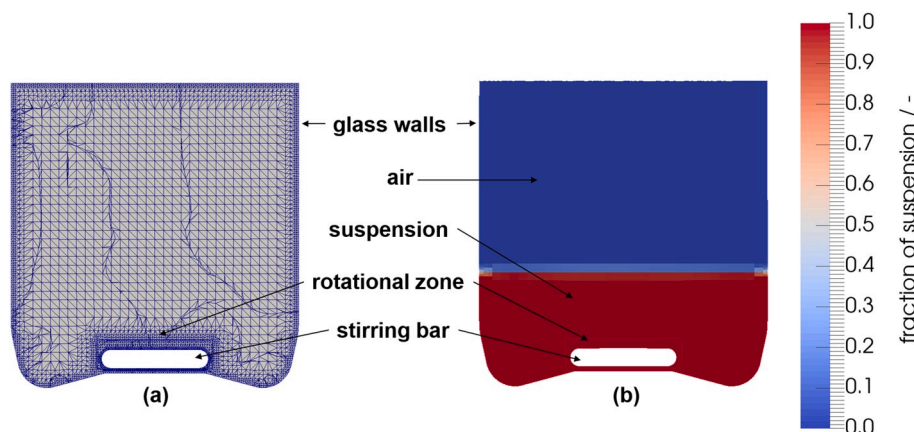


Fig. 1. Meshing (a) and general geometrical setup of the CFD simulation (b).

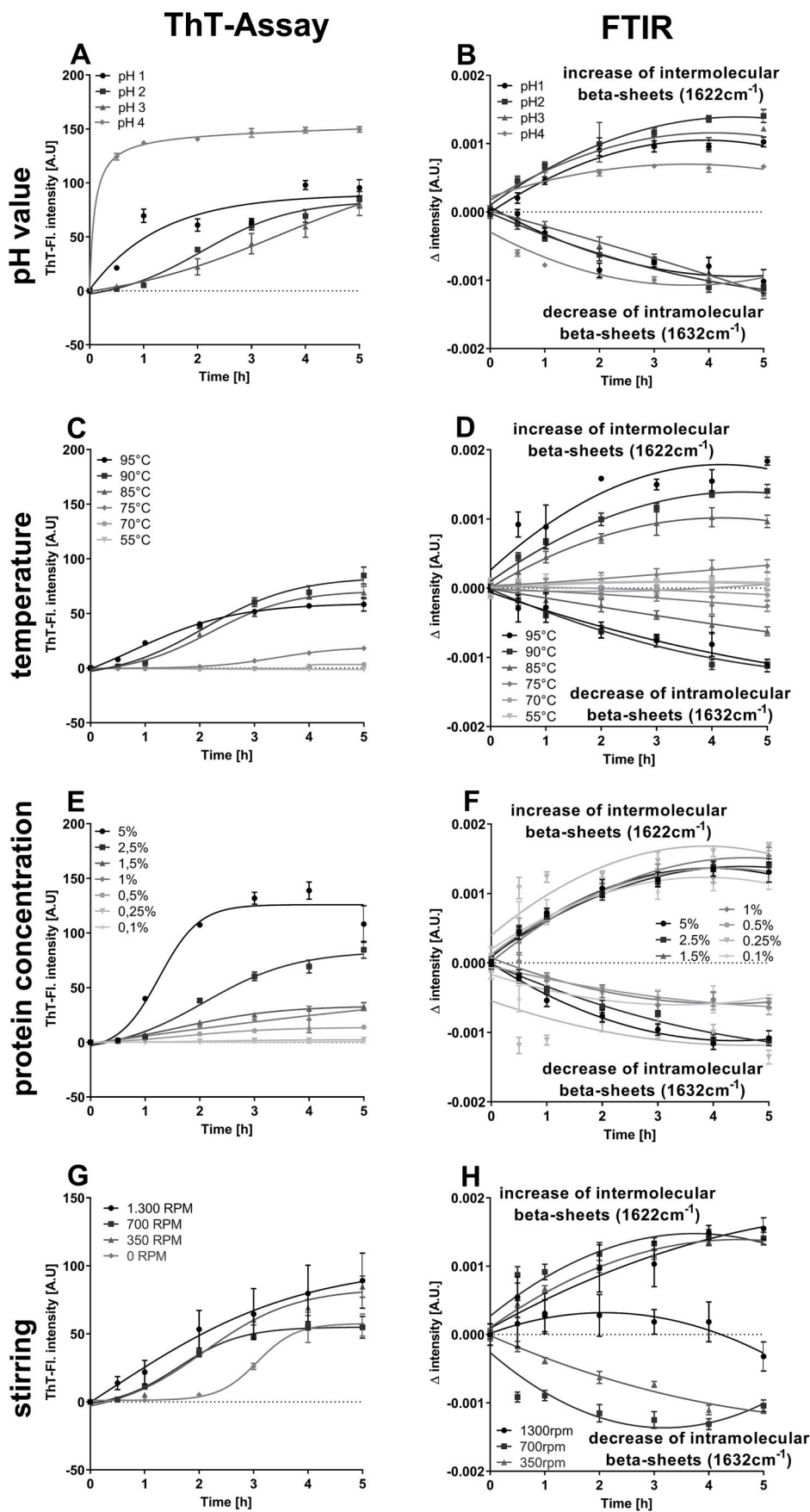


Fig. 2. Influence of pH values (A and B), temperature (C and D), protein concentration (E and F) and stirring velocity (G and H) on Thioflavin-T-fluorescence (ThT FL) and beta-sheet alteration (FTIR) during the first 5 h of fibril production. For improved visibility, a sigmoidal (ThT FL) or a second-order polynomial (FTIR) fitting of measurement points was conducted. Standard process parameters were pH 2, 90 °C heating temperature, 2.5 wt% protein concentration, 350 RPM stirring and 0 mM NaCl.

concentration also excludes effects caused by the viscoelasticity of more concentrated protein solutions. Concentrations lower than 1 wt% were not possible due to the detection limit of the utilised methods. Moreover, the addition of NaCl up to 15 mM showed no effect on amyloid aggregation; therefore the chosen threshold was between 0 and 10 mM. Higher stirring speed (between 350 and 1300 RPM) increased the aggregation kinetics—especially at the beginning of the process at pH 2 and 90 °C (Fig. 2G and H). The stirring speed range of 200–300 RPM was chosen since stirring speeds greater than 300 RPM resulted in increasing air intake (Fig. 6) while stirring speed lower than 200 RPM did not result in a continuous circulation.

The described screening results are mostly in agreement with other observations on pH value (Jung et al., 2008; Krebs et al., 2009; Loveday et al., 2011; Serfert et al., 2014), ion concentration, temperature (Loveday et al., 2011), protein concentration (Schleeger et al., 2013) and stirring speed (Ng et al., 2016).

3.2. Statistical experimental design

The 2⁵ factorial design was conducted via 35 randomised experiments using the threshold parameters determined in the screening experiments (Table 2). The amyloid aggregation was measured by several different methods, called “responses”: ThT-assay (responses “*ThT FL t0.5*” – *t5*), centrifugal ultrafiltration (response “*fibril yield*”), FTIR (response “*Delta 1632 cm⁻¹*” and “*Delta 1622 cm⁻¹*”) and zeta potential (response “*zeta potential*”). In addition, the ThT FL data from six time points over 5 h of incubation were fitted by non-linear regression and the correlation coefficient (*R*²) was taken (response “*regression fitting*”).

The limit of quantification for the ThT-assay was 1.58 a.u., while 0.73 a.u. was the limit of detection. As illustrated in Fig. 2, the level of ThT FL—even just above the detection limit—was a suitable value to describe the formation of fibrils. Analysis with centrifugal ultrafiltration and FTIR did not reach detection limits in most of the cases and were only listed as supportive results for ThT-assay. Nevertheless, the observed secondary structural responses correlated well with the ThT FL results: Intramolecular beta sheets (*Delta 1632 cm⁻¹*) decreased (correlation factor (cf): 0.332) and intermolecular beta sheets (*Delta 1622 cm⁻¹*) increased (cf: 0.301) when the *ThT FL t5* increased. In addition, the fibril yield was also positively correlated with *ThT FL t5* (cf: <0.603).

Consideration of the time factor during the process (only ThT-assay) showed an initial decrease in ThT FL for all experiments, followed by an increase after 3 h and a maximum average value of 2.69 ± 2.66 a.u. after 5 h. If only runs with a high temperature (75 °C) were considered, the initial ThT FL decrease was even lower and the first significant increase was already reached after 2 h (instead of 3 h), while a maximum ThT FL of 5.07 ± 2.02 a.u. occurred after 5 h. When only runs with a low temperature factor (70 °C) were considered, only weak

significant differences were observed after 5 h processing.

The pH value (factor A) influenced the *regression fitting* in a negative manner (calculated coefficient (cc): 0.071) (Table 3). Furthermore, the intramolecular beta sheets (*Delta 1632 cm⁻¹*) seemed to increase at higher pH values (cc: 0.432).

The temperature (factor b) showed the strongest influence on most responses (Table 3). A significant positive temperature-dependent effect was evident for the ThT FL after 3, 4 and 5 h incubation (cc: 0.393 to 0.622) (e.g. Run2 (ThT FL: 8.9 ± 0.62 a.u.), Run7 (ThT FL: 7.9 ± 0.61 a.u.), Run31 (ThT FL: 7.3 ± 0.61 a.u.) and Run17 (ThT FL: 7.1 ± 0.62 a.u.)): all of these runs were at a high temperature level (75 °C). All runs with a temperature equal to or above 75 °C were quantifiable. It has to be assumed that some of the runs at 70 °C also produced fibrils (for example run 23) (Fig. 3). Also, the *regression fitting* (cc: 0.253), *fibril yield* (cc: 1.695), as well as the decrease of intramolecular beta sheets (*Delta 1632 cm⁻¹*) (cc: 0.603) were influenced by temperature (Fig. 4 A to C).

The ion concentration (Factor D) affected the increase of intermolecular beta sheets (*Delta 1622 cm⁻¹*) (cc: 2.589), while the *zeta-potential* was negatively (cc: 1.383) influenced (Table 3).

No significant effects on any response were detected for the protein concentration (Factor C) or the stirring speed (Factor e).

The pH value showed no effect on the threshold of fibril formation as a single factor, however the response of *ThT FL t5* was influenced by the pH value in combination with the temperature (cc: 0.196) (Interaction Factor Ab) (Table 3). This interaction occurred at high temperature levels (75 °C) and led to higher ThT values at lower pH value levels (pH 2.5) (Fig. 4 G).

Another interaction was observed between the stirring speed and the temperature (Interaction Factor be), which influenced the ThT FL in the first 2 h (cc: 0.219 to 0.238) (Table 3). At low stirring speed (200 RPM) ThT FL was negatively affected with increasing temperature, while exhibited a positive effect at high stirring speed (300 RPM) (Fig. 4 D to F).

Since amyloid aggregation and the associated ThT FL increase were related to a shift from the intramolecular to the intermolecular beta-sheets (Heyn et al., 2019), the correlation effect between fibril yield, ThT-assays and FTIR results is explainable.

Observation of the ThT FL during the incubation period showed a decrease in the first 2 h compared to the initial sample (*t0* = native BLG). Notably, a detectable amyloid aggregation did not occur until the third hour of the process. This indicates conformational changes of the native BLG being accompanied by a lower binding capacity of the ThT molecule at the beginning of the process (Krebs et al., 2005). This can include the unfolding as well as the accompanying hydrolysis of the protein (Mishra et al., 2007). Therefore, the first 2 h of the present experiment can be considered the preparatory lag phase of the process. The process then enters into the growth phase, in which the nucleus begins to grow

Table 3

Coefficient table of the statistical experimental design of significant factor-response combinations.

Responses	Intercept	Factors					Factor interactions	
		A	b	C	D	e	Ab	be
<i>ThT FL int. t0.5</i>	-0.198		-0.057 ^c			0.065 ^c		0.219 ^b
<i>ThT FL int. t1</i>	-0.178		-0.069 ^c			0.068 ^c		0.222 ^b
<i>ThT FL int. t2</i>	-0.087		0.071 ^c			0.125 ^c		0.238 ^b
<i>ThT FL int. t3</i>	0.293		0.393 ^a			0.119 ^c		0.216 ^c
<i>ThT FL int. t4</i>	1.598	-0.107 ^b	0.391 ^a			0.044 ^c	-0.159 ^a	0.024 ^c
<i>ThT FL int. t5</i>	1.866	-0.111 ^c	0.622 ^a			0.087 ^c	-0.196 ^a	-0.0115 ^c
<i>Regression fitting</i>	0.579	-0.071 ^a	0.253 ^a			0.034 ^c		-0.058 ^c
<i>Fibril yield</i>	5.235		1.695 ^a			0.367 ^c		0.281 ^c
<i>Delta 1632 cm⁻¹</i>	4.037	0.432 ^b	-0.603 ^a	0.003 ^c	-0.095 ^c	-0.158 ^c		0.049 ^c
<i>Delta 1622 cm⁻¹</i>	3.108		1.203 ^c		2.589 ^a	1.386 ^c		0.566 ^c
<i>Zeta potential</i>	24.008				-1.383 ^b			

Significance level of calculated coefficient: ^a p < 0.05, ^b: p < 0.10, ^c p ≥ 0.10.

Factors: pH-value (A), temperature (b), protein concentration (C), NaCl concentration (D), stirring velocity (e).

ThT FL int.: Thioflavin-T fluorescence intensity.

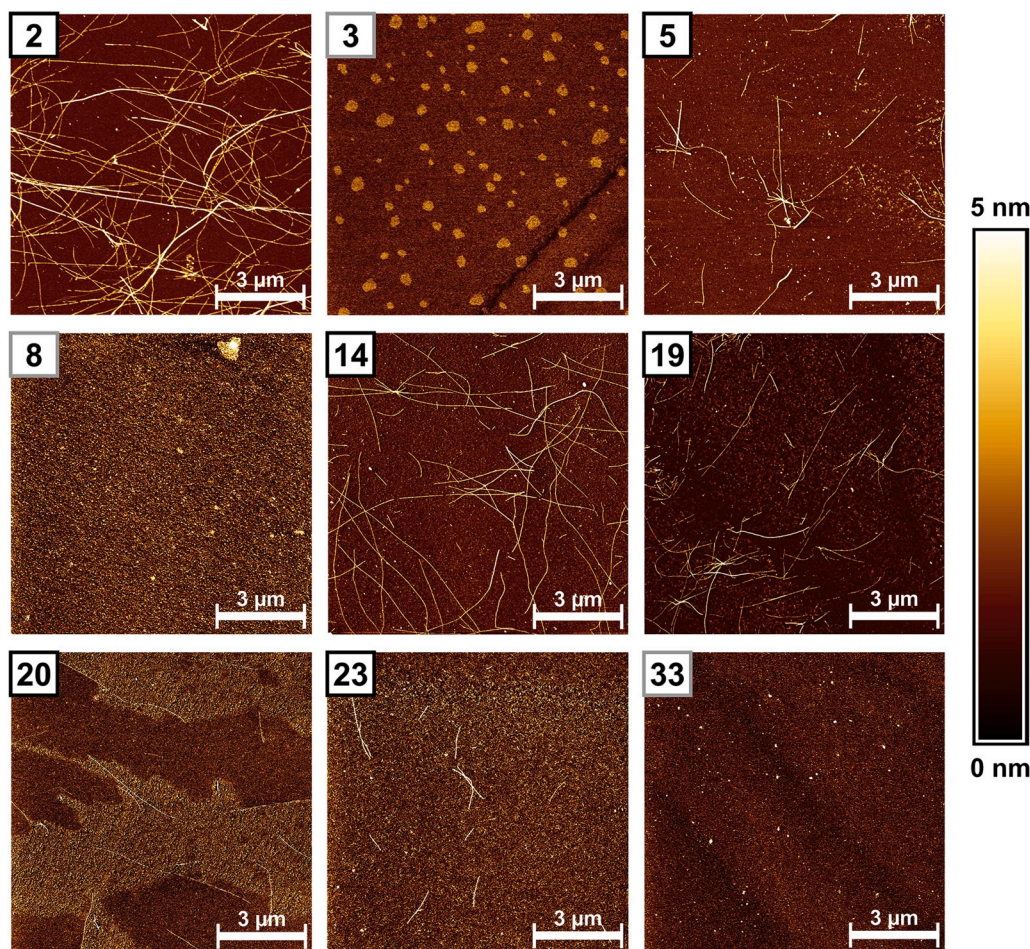


Fig. 3. Atomic force microscopy images of samples with 0.01 wt% protein. Factor combinations leading to fibril formation (black border): Run2 (ThT FL: 8.899 a.u.); Run5 (ThT FL: 2.841 a.u.); Run14 (ThT FL: 6.74 a.u.); Run19 (ThT FL: 2.84 a.u.); Run23 (ThT FL: 1.633 a.u.); Centre point Run20 (ThT FL: 1.419 a.u.); Runs without fibril formation (grey border): Run3 (ThT FL: 0.229 a.u.); Run8 (ThT FL: 0.578 a.u.); Run33 (ThT FL: 0.350 a.u.).

above a detectable size (Loveday et al., 2017). That these phases can be reached slower or faster, depending on the temperature, has already been described (Loveday et al., 2012b). The initiation phase is considerably extended due to the selected low factor values. Therefore, the present experimental setup at the threshold to amyloid aggregation can be regarded as a closer look into the lag and initial stages of the growing phase of amyloid aggregation. Notably, that the observed factor combinations at different time points are either strong effects that influence the aggregation process in a timely manner—and can thus be directly assigned to the different phases of amyloid aggregation—or weak effects that accumulate slowly and reach a significant intensity with delay.

First and primarily, an effect of temperature on fibril formation was observed during the growing phase (≥ 3 h). This is a confirmation of the hypothesis that temperature might be an important factor for the denaturation of BLG, its hydrolysis rate and/or the aggregation kinetics of the building blocks. This question is investigated and discussed in greater detail in Part 3.3.1.

After 4 h, an interaction between the pH value and temperature was observed, with a stronger amyloid aggregation at lower pH values. This effect opposes the increased electrostatic repulsion at lower pH values (Bhattacharjee, 2016; Gilbert et al., 2014; Krebs et al., 2009). The lower pH value had a decreasing effect on the required denaturing temperature of the protein and thus accelerated the amyloid aggregation. This question is investigated in Part 3.3.2 with the help of a DSC investigation. A similar interaction at higher temperatures and more acidic pH values (between pH 1.5 and 2.5) than applied in the present experiments was described by (Loveday et al., 2011). The observed interaction could

be explained by the temperature and pH-dependent kinetics of hydrolysis and the associated supply of fibril building blocks (Kroes-Nijboer et al., 2011). However, no pH-dependent threshold shift can be derived from this since the effect only occurs at higher temperatures.

Another effect that influences the ThT FL during the lag phase (i.e. below 3 h incubation here) was stirring speed in the incubation glass vessel in combination with temperature. Notably, both factors influence particle movement in the solution. In addition to the temperature-dependent effect, a shear-dependent effect may also play a role in protein conformation (Rahaman et al., 2015). These effects are investigated in greater detail in Part 3.3.3 via CFD simulation.

As expected, zeta potential decreased due to increased ion concentration (Bhattacharjee, 2016). The increase of intermolecular beta-sheets ($\sim 1622 \text{ cm}^{-1}$) is described in the literature in the course of amyloid aggregation (Baldassarre et al., 2016; Kavanagh et al., 2000). The positive effect of NaCl concentration on the intensity increase of this secondary structure can be attributed to the neutralisation of repulsive electrostatic interactions by Na^+ ions (Bryant and McClements, 2000).

3.2.1. Influence of temperature on amyloid aggregation

To determine whether the temperature is only crucial in the first stage but not in the later stages of fibril growth, the standard heating protocol was changed after a defined period of time. Therefore, the temperature was lowered from 90 °C to either 30 °C or 60 °C after 2 h and 3 h, while all other parameters were maintained.

As presented in Fig. 5, the ThT FL in the process of fibril formation at 90 °C reached an intensity of 38.2 ± 7.1 a.u. after 2 h and 53.9 ± 1.3 a.u.

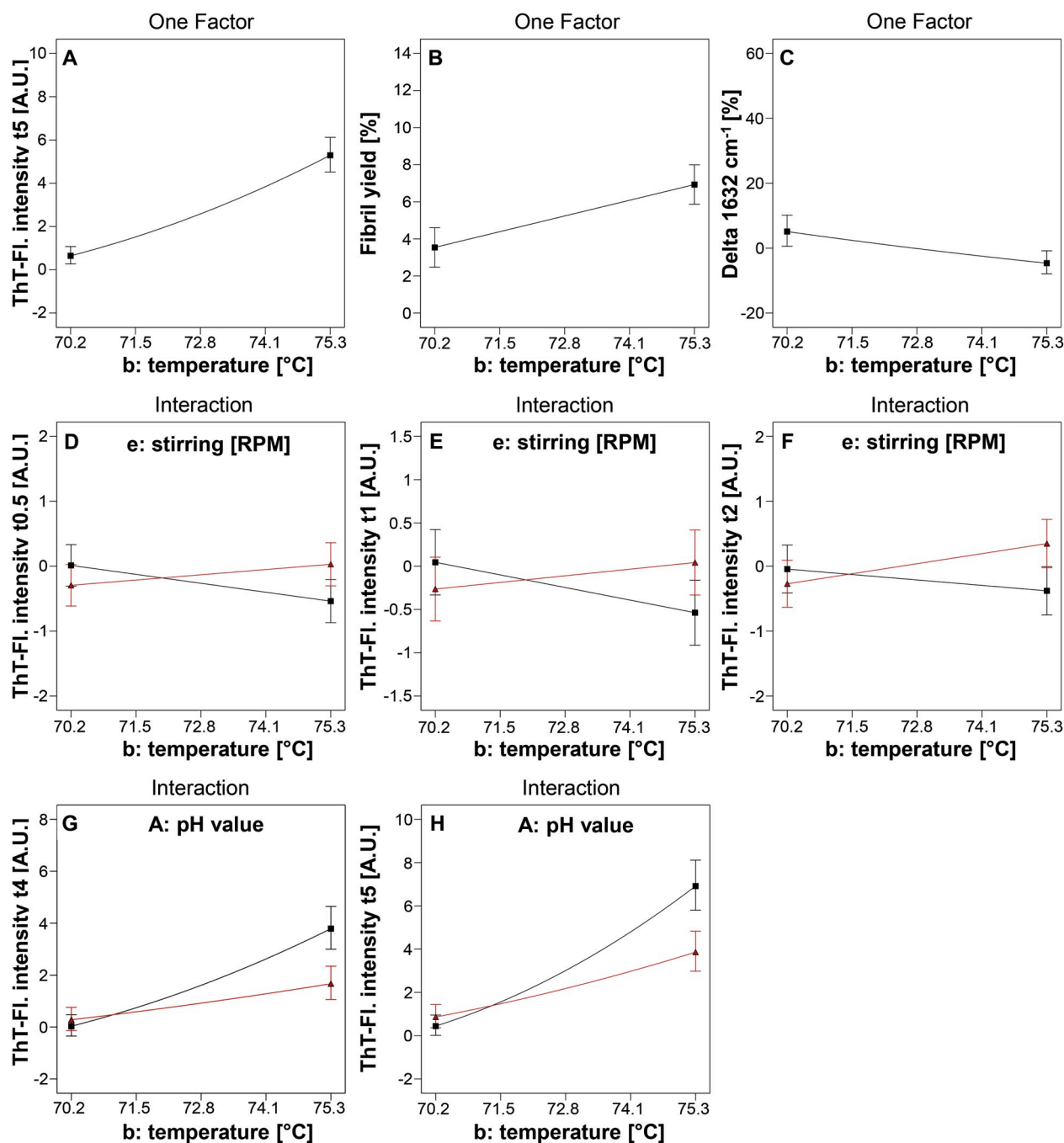


Fig. 4. Influence of temperature on Thioflavin-T-fluorescence (ThT FL) after 5 h (A), fibril yield (B) and intramolecular beta sheets (C) at pH 2.75, 1.25 wt% protein concentration, 5 mMol NaCl and 250 RPM stirring. Interaction of stirring*temperature as an influencing factor on ThT FL t0.5 (D), t1 (E) and t2 (F). Stirring at 300 RPM (Δ) and 200 RPM (\square) (Other parameters are pH 2.75, 1.25 wt% protein concentration and 5 mMol NaCl). Interaction of pH value*temperature (Ab) to influence ThT FL t4 (G) and t5 (H). pH 3 (Δ) and pH 2.5 (\square) (Other parameters are 1.25 wt% protein concentration, 5 mMol NaCl concentration and 250 RPM stirring velocity). The curve between Level 1 and Level 2 values is hypothetical and the respective curvature was calculated using the position of the centre points.

after 3 h (Fig. 5). If the temperature was lowered to 30 or 60 °C at the respective time points, the ThT FL increase (k_{ThT}) was significantly lower with $\Delta \ln k_{\text{ThT}} = -3.7$ (30 °C) and $\Delta \ln k_{\text{ThT}} = -2.1$ (60 °C) compared to 90 °C in the two scenarios. Furthermore, SEC analysis illustrates that the loss of BLG through hydrolysis was followed by a decreasing exponential function, as previously described by (Kroes-Nijboer et al., 2011). The level of hydrolysis reached ~30% after 2 h and ~41% after 3 h. Moreover, the temperature reduction to 30 °C led to a decrease in the hydrolysis rate by $\Delta \ln k_h = -6.63$ compared to 90 °C, while at 60 °C a hydrolysis rate of $\Delta \ln k_h = -2.89$ was calculated by the Arrhenius equation described by (Kroes-Nijboer et al., 2011).

The results indicate that the fibril formation process was interrupted by a temperature drop regardless of the incubation time. The strong influence of temperature on amyloid aggregation during the initiation phase was highlighted by the fact that protein denaturation—and thus acid hydrolysis—was induced. However, the irreversible denaturation of BLG at 90 °C might be completed in the first few hours of the process (Keppler et al., 2014; Loveday, 2016), so that the reduced fibril formation after temperature reduction was not likely caused by reduced denaturation. However, temperature strongly affects the hydrolysis rate and thus the availability of fibril building blocks (hydrolysed/peptide material) (Kroes-Nijboer et al., 2011; Ye et al., 2018).

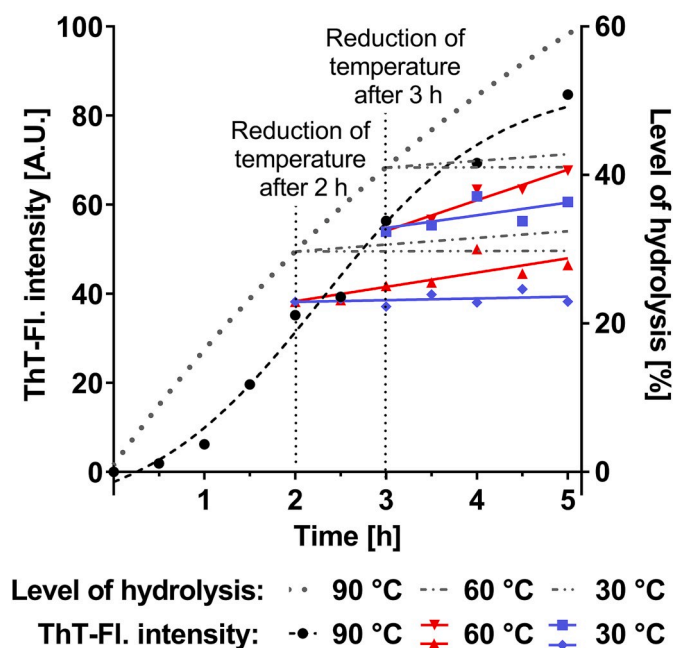


Fig. 5. ThT-assays of fibril formation (90 °C, pH 2, 350 RPM) with a temperature drop after 2 h or 3 h and continuation of the process at 30 °C or 60 °C (pH 2, 350 RPM) until a total of 5 h was reached. For improved visualization the ThT FL at 90 °C was fitted with a sigmoidal logarithmic equation, while ThT FL at 30 °C and 60 °C were fitted with a linear equation. The level of hydrolysis was measured by size exclusion chromatography and fitted with an exponential plateau equation. Hydrolysis rates were calculated using the Arrhenius equation given by Kroes-Nijboer et al. (2011).

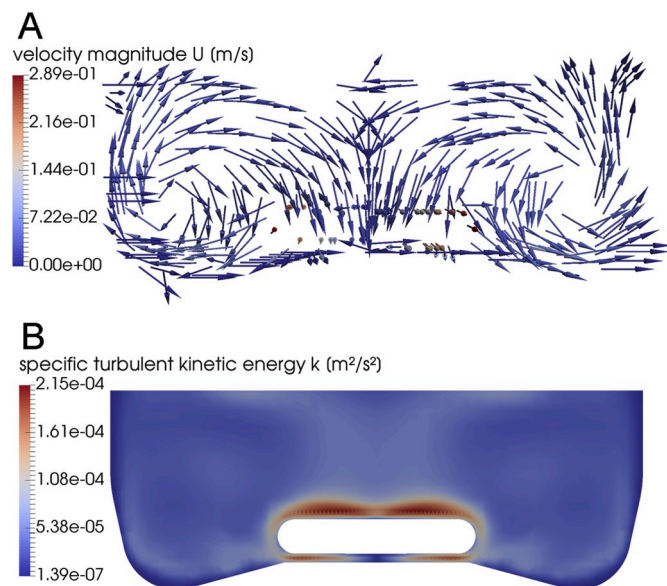


Fig. 6. The resulting flow pattern (A) and specific turbulent kinetic energy (B) for the simulation of 300 RPM at 70 °C and t_0 in the section of the suspension domain in the y-direction after 1.90 s of simulation time.

According to the measured hydrolysis level (i.e. after 2 h = ~30%, after 3 h = ~41%) (Fig. 5), as well as our previous studies on the amount of peptides that are incorporated into the fibrils (i.e. after 2 h = ~13%, after 3 h = ~19%) (Heyn et al., 2019) and the amount of peptides required for fibril formation (i.e. after 2 h = ~26%, after 3 h = ~38%) (Keppler et al., 2019) at pH 2 and 90 °C, there seems to be sufficient surplus fibril building blocks available (i.e. after 2 h = ~4%, after 3 h =

~3%) to ensure a further fibril formation of approximately 10 a.u. ThT FL after each temperature drop.

Therefore, it is hypothesised that this instant temperature-dependent decrease is primarily related to the aggregation kinetics and less dependent on the hydrolysis rate. In fact, there was an instant drop in the aggregation kinetics ($\Delta \ln k_{\text{ThT}} = -3.7$ (30 °C) and $\Delta \ln k_{\text{ThT}} = -2.1$ (60 °C)) as soon as the solutions cooled down (Fig. 5). Additionally, the amyloid-like aggregation of BLG is also possible without hydrolysis (for example at pH 3.5 and 90 °C) where the depletion of building blocks is independent of the peptide concentration (Heyn et al., 2019). A further effect of temperature on the entire progression of amyloid aggregation might also include other mechanisms. For example, it is possible that reversible protein conformations are induced by higher temperatures, that lead to amyloid aggregation (Bhattacharjee and Das, 2000). Another possible mechanism could be the dependence of the diffusion coefficient of the protein on temperature (Macchioni et al., 2008), which increases the frequency of molecular collisions and leads to the accelerated formation of aggregates (Wang et al., 2010); however, this would be affected by the turbulence in the system (Part 3.3.3). Another factor is that the dielectric constant of the medium decreases with increasing temperature, which favours interactions between proteins—and thereby amyloid aggregation (Kayser et al., 2020).

However, since the observed acid hydrolysis rate at 30 °C and 60 °C decreased compared to 90 °C ($\Delta \ln k_h = -6.63$ (30 °C), $\Delta \ln k_h = -2.89$ (60 °C)) (Fig. 5), the limiting factor in the long run of the fibril aggregation process will ultimately be a depletion of building blocks, when all available protein is finally hydrolysed, as previously mentioned before by Kroes-Nijboer et al. (2011).

Ultimately, several overlapping mechanisms seem to explain the observed strong positive influence of temperature on amyloid aggregation (Table 3).

3.2.2. Interaction of temperature and pH value

The investigation of a pH-dependent denaturation effect was performed by DSC. The 1 wt% BLG samples were adjusted to pH values of 2.0, 2.5 and 3.0 to achieve parameters similar to those in the statistical experiment.

Samples were heated to 110 °C at 5 °C min⁻¹ and cooled to 20 °C at 20 °C min⁻¹. Notably decreasing energy absorption of the BLG solution at increasing pH values (below the isoelectric point: $pI = 4.7$) during heat development was observed: At pH 2.0, the denaturation enthalpy was 448.13 ± 8.37 kJ mol⁻¹, while at pH 2.5 it was 288.68 ± 29.44 kJ mol⁻¹ and at pH 3.0 it was 226.58 ± 31.63 kJ mol⁻¹ (Table 4).

Simultaneously, the threshold of BLG denaturation increased with increasing pH value. At pH 2, the onset temperature was ~72 °C, while at pH 2.5 it was ~80 °C and at pH 3.0 it was ~82 °C (Table 4). The maximum denaturation for BLG was reached at a pH value of 2.0 at ~84 °C, while this was observed at pH 2.5 at ~86 °C and at pH 3.0 at ~90 °C (Table 4).

The results indicate that the denaturation of BLG depended on pH values being below the isoelectric point. As previously described by (Haug et al., 2009), the temperature at which BLG begins to denature increases with increasing pH value in an acidic environment. Variations in the literature (Griko and Privalov, 1992; Kella and Kinsella, 1988; Wada et al., 2006; Wit and Swinkels, 1980) can be explained by the utilised methods and the dependence of denaturation enthalpy and temperature on other factors such as protein and ion concentration

Table 4

Differential scanning calorimetry (DSC) of beta-lactoglobulin (1 wt%) at pH 2.0, 2.5 and 3.0.

pH value	Enthalpy [kJ mol ⁻¹]	Onset [°C]	Peak [°C]
pH 2.0	448.13 ± 8.37	71.95 ± 0.10	84.32 ± 0.80
pH 2.5	288.68 ± 29.44	79.89 ± 0.41	86.01 ± 0.16
pH 3.0	226.58 ± 31.63	82.14 ± 0.17	90.24 ± 0.57

(Dissanayake et al., 2013). In combination with the pH value, protein and ion concentrations influence the BLG monomer/dimer equilibrium, while dimers or multimers were subsequently found to stabilise the native structure of BLG and thus affect the denaturation temperature (Haug et al., 2009; Renard et al., 1998).

The present results prove that a pH value shift from pH 3.0 to pH 2.5 already leads to a reduction in temperature, which is required for the protein to unfold. It could be speculated that increased reversible conformational changes (Bhattacharjee and Das, 2000) can influence the rate of aggregation, as fibrillation prone peptide segments become accessible (van der Linden and Venema, 2007). Thus, if the pH makes the protein more prone to denaturation and the aggregation kinetics depend directly on the protein conformation, this effect would shift the threshold of amyloid aggregation. However, the lower thermal stability of BLG at lower pH values not only increases the unfolding of the protein, but acid hydrolysis at lower pH values is also favoured, which is an additional factor that amplifies together with temperature (see Part 3.3.1). Since this effect only led to increased ThT-values at high temperature (Fig. 4 G and H), and no shift of the amyloid aggregation threshold occurred, a direct effect of denaturation on aggregation kinetics is less conceivable.

3.2.3. Influence of fluid dynamics on amyloid aggregation

In Fig. 6, it can be observed that the region with the highest velocities—and thus the highest strain on the proteins—was located at the tips of the stirring bar. The energy input of the stirring bar drove the suspension outwards along the bottom of the glass container, where it finally flowed upwards at the outer edge of the glass container and then back towards the stirrer in the middle of the glass container due to the conservation of mass (Fig. 6 A). This results in large flow vortices in which the proportion of turbulence also varies (Fig. 6 B), thereby resulting in variance in both turbulent and laminar flow. This results in small areas with high shear and large areas with low shear, which can lead to uneven stress distribution of the suspension—and thus of the proteins as well. The distribution of the shear stress in the system may have the same effect of causing short time impulses in a small volume, thereby interrupting the laminar flow. Thus, the intense but short mechanical stress impulses over the small area around the stirrer (Fig. 6) can lead to the obligatory unfolding of the protein (Dunstan et al., 2009) or to a fracture of protofibrils to seeds (Hill et al., 2006), whereby a primary or secondary nucleation of the building blocks can occur in the large areas with low laminar stress (Akkermans et al., 2008a). The aggregation-accelerating effect of 30 s shear pulses has been previously described (Akkermans et al., 2006). This simulation clearly presents fibril growth accelerating (Fig. 2 G) shear heterogeneity in the chosen parameter range in a stirred glass container (Bolder et al., 2007).

As shown in Table 3, significant interactions between temperature and stirring speed occurred, which positively influence amyloid aggregation (i.e. ThT FL increase). The CFD model used here calculates the averaged mean and maximum shear stresses during the simulated stirring time, shear rate, turbulence eddy dissipation (ϵ) and energy (k) in the turbulence model, depending on temperature, viscosity and stirring speed. The viscosity depends on the degree of aggregation, protein concentration and temperature, and was specifically determined for time points t0 and t5 using a shear rheometer at a protein concentration of 1.25 wt%.

The consideration of all flow-dependent parameters show an increase as a function of stirring speed; for example, a mean shear stress of t0 at 70 °C increase from 0.040 ± 0.001 Pa to 0.064 ± 0.002 (Fig. 7 A), the mean shear rate from 50.1 ± 1.6 s⁻¹ to 79.7 ± 2.4 s⁻¹ (Fig. 7 C) and the mean turbulence eddy dissipation from 0.0008 ± 0.0002 to 0.0019 ± 0.0016 (Fig. 7 E). Stirring speed-dependent increases in shear stress, shear rate and turbulence were also observed for the maximum values (Fig. 7 B, D and F).

Although, significant Pearson correlations between the stress factors (shear stress, shear rate, epsilon and k) and the measured ThT FL t0.5 to

t5 were not observed, relatively high r-values were evident between shear stress and ThT FL from time t2. Additionally, a temperature-dependent increase was only achieved with rising shear stress. At t0, 200 RPM and 75 °C the mean shear stress increased to 0.067 ± 0.002 Pa, while it increased to 0.108 ± 0.004 Pa at 300 RPM. A similar increase was also observed at the maximum values. However, it should be noted that this temperature-dependent increase was lost after 5 h. The reason for this is the dependency of the shear stress on the respective viscosity:

$$\tau = \eta \cdot \dot{\gamma}$$

where $\dot{\gamma}$ is the shear rate and η is the dynamic viscosity. As listed in Table 5, the t0 sample had a dynamic viscosity of 0.8 mPa s at 70 °C and rose to 1.5 mPa s at 75 °C. For the t5 sample, the viscosity at 70 °C increased only slightly from 1.1 mPa s to 1.2 mPa s. The lower viscosity of the sample (although heated for 5 h) can be explained by the shear-thinning behaviour of the fibrillary component in the t5 sample.

Effects being detected mainly during the lag phase of the process could be an indication that the shear stress exerts an effect on the conformation of the unhydrolysed BLG (Rahaman et al., 2015), already described a shear-dependent reduction of the hydrophobicity of BLG at pH3 and a resulting increased polymerisation and compactness to which the ThT could react.

The shear-induced effect on protein conformation would thus have the potential to influence the threshold of amyloid aggregation. However, the ThT FL values during the growth phase showed no further stirring-dependent effects. Perhaps the shear difference between the two levels was insufficient for the detection of further effects. Another reason could be that the increasing viscosity counteracts protein aggregation: either by lower particle diffusion or because the associated increased shear stress disrupts the forming nucleus again (Akkermans et al., 2006; Dunstan et al., 2009). However, as described in Part 3.3.2, an irreversible change in protein conformation or denaturation may not be responsible for amyloid aggregation alone.

4. Conclusion

The present experimental parameters were chosen to prolong the lag and growth phase of the amyloid aggregation and thus give evidence for important processing parameters at the onset of amyloid aggregation. The experiments presented indicate that, at the threshold of fibril formation, partly different interaction effects can occur than at the optimum: however, the most important factor is the temperature in every stage of amyloid aggregation, which could be due to manifold effects that superpose each other. This is also confirmed by further interactions between stirring speed and temperature during the lag phase and between pH and temperature during the growth phase.

With the help of a CFD simulation of the stirring process, higher shear stress at higher stirring speeds and temperatures could be identified as the reason for the interaction, which likely negatively affects the protein nativity and thus reduces the lag phase. The increased viscosity of the protein solution at higher temperatures likely plays a major role in this interaction.

The effect of pH value and temperature in the growth phase could be explained by DSC experiments, which revealed that BLG was more likely to denature at pH 2.5 than at pH 3.0 for the selected factor combinations.

Thus, each of the chosen process parameters affects the underlying forces of amyloid aggregation in multiple and sometimes opposing ways, while only the sum of the effects can be observed here at a certain point in the amyloid aggregation phase.

Due to the very slow aggregation kinetics of the selected parameters, the investigations provide a more detailed view of the most important factors and when they come into effect. Meanwhile, new interactions could also be described. These do not seem to shift the threshold; however, it is conceivable that other and more extreme factor

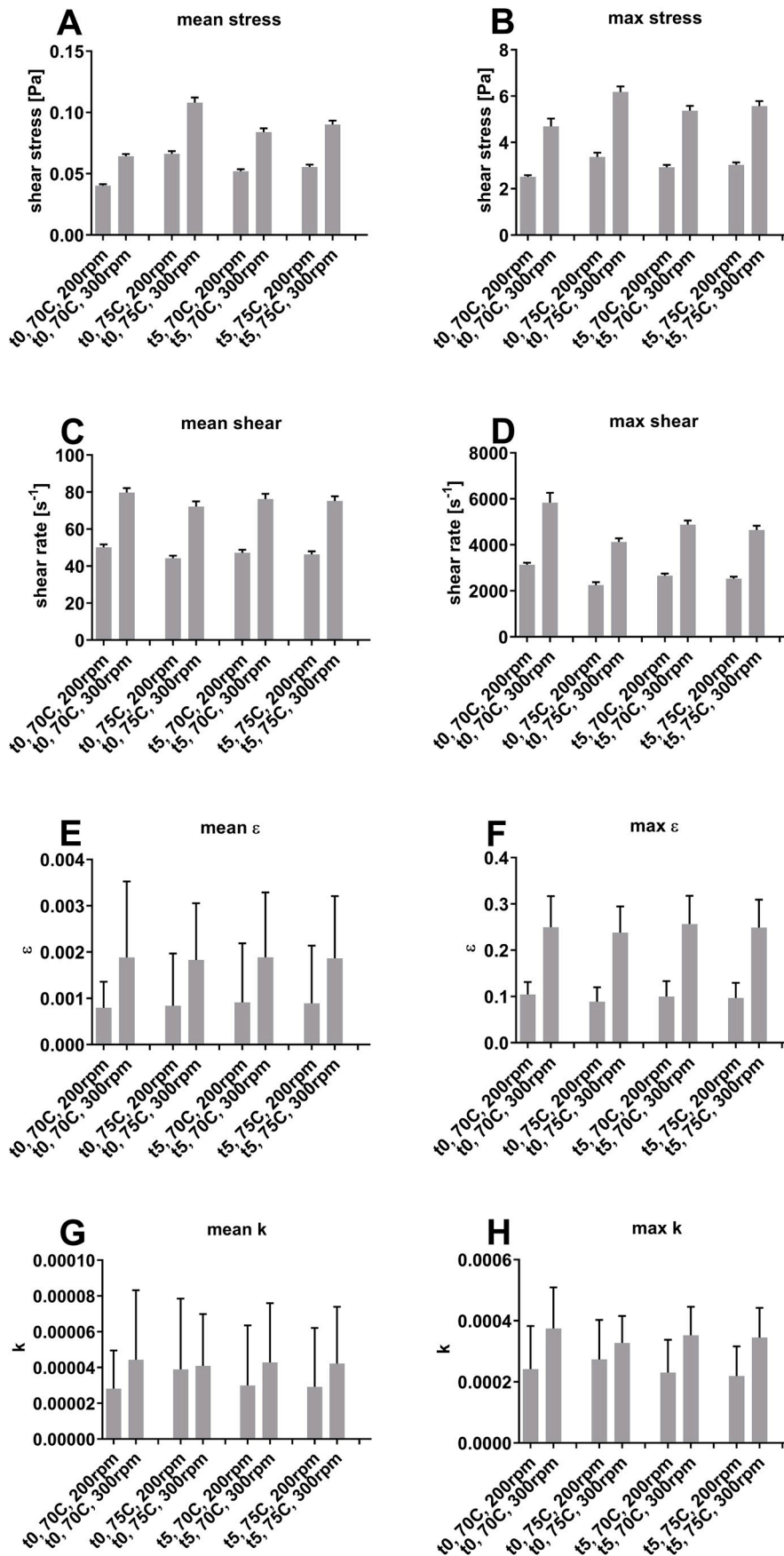


Fig. 7. Stress factors in the stirring container during 5 h of fibril formation calculated via CFD simulation. Sample viscosity was determined at each time point using a shear rheometer. k describes the turbulence kinetic energy. ϵ describes the rate of dissipation of turbulence energy.

Table 5

Viscosity data used for computational fluid dynamics (CFD) simulations.

	Kinematic viscosity [m ² s ⁻¹]	Density [kg m ⁻³]	Dynamic viscosity [mPas]
t0, 70 °C:	0.80E-06	1001.33	0.80
t0, 75 °C:	1.50E-06	998.44	1.50
t5, 70 °C:	1.10E-06	1001.33	1.10
t5, 75 °C:	1.20E-06	998.44	1.12
Air	15.35E-06	1.188	0.02

combinations might decrease the necessary temperature under 70 °C.

Declaration of competing interest

None.

CRediT authorship contribution statement

Timon R. Heyn: Conceptualization, Methodology, Formal analysis, Investigation, Validation, Visualization, Writing - original draft. **Julian Mayer:** Software, Methodology, Investigation, Writing - original draft, Visualization. **Hendrikje R. Neumann:** Methodology, Investigation. **Christine Selhuber-Unkel:** Resources, Writing - review & editing. **Arno Kwade:** Resources, Writing - review & editing. **Karin Schwarz:** Funding acquisition, Resources, Writing - review & editing, Supervision. **Julia K. Keppler:** Project administration, Funding acquisition, Conceptualization, Resources, Supervision, Writing - review & editing.

Acknowledgement

The authors gratefully acknowledge the financial support provided by the German Research Foundation (DFG) within the priority program, SPP1934 "DiSPBiotech – Dispersity, structural and phase modifications of proteins and biological agglomerates in biotechnological processes" (Project no. 273937032 and 315456892). We are grateful to Monique Heuer and Jil J. Kayser of the Food Technology Division, Kiel University for their skilfull help with the DOE experiments and we acknowledge the professional technical work of Maurice Strubel of the Department of Agrotechnology and Food Sciences, Wageningen University in conducting the DSC analysis.

Appendix A. Supplementary data

Supplementary data to this article can be found online at <https://doi.org/10.1016/j.jfoodeng.2020.110005>.

References

Akkermans, C., van der Goot, A.J., Venema, P., van der Linden, E., Boom, R.M., 2008a. Formation of fibrillar whey protein aggregates. *Food Hydrocolloids* 22 (7), 1315–1325. <https://doi.org/10.1016/j.foodhyd.2007.07.001>.

Akkermans, C., Venema, P., Rogers, S.S., van der Goot, A.J., Boom, R.M., van der Linden, E., 2006. Shear pulses nucleate fibril aggregation. *Food Biophys.* 1 (3), 144–150. <https://doi.org/10.1007/s11483-006-9012-5>.

Akkermans, C., Venema, P., van der Goot, A.J., Gruppen, H., Bakx, E.J., Boom, R.M., et al., 2008b. Peptides are building blocks of heat-induced fibrillar protein aggregates of beta-lactoglobulin formed at pH 2. *Biomacromolecules* 9 (5), 1474–1479. <https://doi.org/10.1021/bm7014224>.

Arnaudov, L.N., Vries, R. de, 2006. Strong impact of ionic strength on the kinetics of fibrillar aggregation of bovine beta-lactoglobulin. *Biomacromolecules* 7 (12), 3490–3498. <https://doi.org/10.1021/bm060584i>.

Baldassarre, M., Bennett, M., Barth, A., 2016. Simultaneous acquisition of infrared, fluorescence and light scattering spectra of proteins. *Analyst* 141 (3), 963–973. <https://doi.org/10.1039/c5an02283e>.

Bhattacharjee, C., Das, K.P., 2000. Thermal unfolding and refolding of beta-lactoglobulin. An intrinsic and extrinsic fluorescence study. *Eur. J. Biochem.* 267 (13), 3957–3964. <https://doi.org/10.1046/j.1432-1327.2000.01409.x>.

Bhattacharjee, S., 2016. DLS and zeta potential - what they are and what they are not? *J. Contr. Release* 235, 337–351. <https://doi.org/10.1016/j.jconrel.2016.06.017>.

Bliatsiou, C., Malik, A., Böhm, L., Kraume, M., 2018. Influence of impeller geometry on hydro-mechanical stress in stirred liquid/liquid dispersions. *Ind. Eng. Chem. Res.* 58 (7), 2537–2550. <https://doi.org/10.1021/acs.iecr.8b03654>.

Bolder, S.G., Sagis, L.M.C., Venema, P., van der Linden, E., 2007. Effect of stirring and seeding on whey protein fibril formation. *J. Agric. Food Chem.* 55 (14), 5661–5669. <https://doi.org/10.1021/jf063351r>.

Bryant, C.M., McClements, D.J., 2000. Influence of NaCl and CaCl₂ on cold-set gelation of heat-denatured whey protein. *J. Food Sci.* 65 (5), 801–804. <https://doi.org/10.1111/j.1365-2621.2000.tb13590.x>.

Ciuciu, A.-M.S., Aprodou, I., Alexe, P., Stănciuc, N., 2016. Thermally driven interactions between β-lactoglobulin and retinol acetate investigated by fluorescence spectroscopy and molecular modeling methods. *Dairy Sci. Technol.* 96 (3), 405–423. <https://doi.org/10.1007/s13594-015-0277-7>.

Dissanayake, M., Ramchandran, L., Donkor, O.N., Vasiljevic, T., 2013. Denaturation of whey proteins as a function of heat, pH and protein concentration. *Int. Dairy J.* 31 (2), 93–99. <https://doi.org/10.1016/j.idairyj.2013.02.002>.

Dunstan, D.E., Hamilton-Brown, P., Asimakis, P., Duckler, W., Bertolini, J., 2009. Shear-induced structure and mechanics of β-lactoglobulin amyloid fibrils. *Soft Matter* 5 (24), 5020. <https://doi.org/10.1039/b914089a>.

Dvorsky, R., Sevcik, J., Caves, L.S.D., Hubbard, R.E., Verma, C.S., 2000. Temperature effects on protein motions. *J. Phys. Chem. B* 104 (44), 10387–10397. <https://doi.org/10.1021/jp001933k>.

Einstein, A., 1905. Über die von der molekularkinetischen Theorie der Wärme geforderte Bewegung von in ruhenden Flüssigkeiten suspendierten Teilchen. *Ann. Phys.* 322 (8), 549–560. <https://doi.org/10.1002/andp.19053220806>.

Gao, Z., Zhao, J., Huang, Y., Yao, X., Zhang, K., Fang, Y., et al., 2017. Edible Pickering emulsion stabilized by protein fibrils. Part 1. *LWT - Food Sci. Technol. (Lebensmittel-Wissenschaft -Technol.)* 76, 1–8. <https://doi.org/10.1016/j.lwt.2016.10.038>.

Gilbert, J., Campanella, O., Jones, O.G., 2014. Electrostatic stabilization of β-lactoglobulin fibrils at increased pH with cationic polymers. *Biomacromolecules* 15 (8), 3119–3127. <https://doi.org/10.1021/bm500762u>.

Griko, Y.V., Privalov, P.L., 1992. Calorimetric study of the heat and cold denaturation of beta-lactoglobulin. *Biochemistry* 31 (37), 8810–8815. <https://doi.org/10.1021/bi00152a017>.

Haug, I.J., Skar, H.M., Vegarud, G.E., Langsrud, T., Draget, K.I., 2009. Electrostatic effects on β-lactoglobulin transitions during heat denaturation as studied by differential scanning calorimetry. *Food Hydrocolloids* 23 (8), 2287–2293. <https://doi.org/10.1016/j.foodhyd.2009.06.006>.

Havinga, E.E., 1961. The temperature dependence of dielectric constants. *J. Phys. Chem. Solid.* 18 (2–3), 253–255. [https://doi.org/10.1016/0022-3697\(61\)90169-X](https://doi.org/10.1016/0022-3697(61)90169-X).

Heyn, T.R., Garamus, V.M., Neumann, H.R., Uttinger, M.J., Guckeisen, T., Heuer, M., et al., 2019. Influence of the polydispersity of pH 2 and pH 3.5 beta-lactoglobulin amyloid fibril solutions on analytical methods. *Eur. Polym. J.* 120, 109211. <https://doi.org/10.1016/j.eurpolymj.2019.08.038>.

Hill, E.K., Krebs, B., Goodall, D.G., Howlett, G.J., Dunstan, D.E., 2006. Shear flow induces amyloid fibril formation. *Biomacromolecules* 7 (1), 10–13. <https://doi.org/10.1021/bm0505078>.

Jung, J.-M., Savin, G., Pouzot, M., Schmitt, C., Mezzenga, R., 2008. Structure of heat-induced beta-lactoglobulin aggregates and their complexes with sodium-dodecyl sulfate. *Biomacromolecules* 9 (9), 2477–2486. <https://doi.org/10.1021/bm800502j>.

Kavanagh, G.M., Clark, A.H., Ross-Murphy, S.B., 2000. Heat-induced gelation of globular proteins. *Langmuir* 16 (24), 9584–9594. <https://doi.org/10.1021/la0004698>.

Kayser, J.J., Arnold, P., Steffen-Heins, A., Schwarz, K., Keppler, J.K., 2020. Functional ethanol-induced fibrils. *J. Food Eng.* 270, 109764. <https://doi.org/10.1016/j.jfoodeng.2019.109764>.

Kella, N.K., Kinsella, J.E., 1988. Enhanced thermodynamic stability of beta-lactoglobulin at low pH. A possible mechanism. *Biochem. J.* 255 (1), 113–118. <https://doi.org/10.1042/bj2550113>.

Keppler, J.K., Heyn, T.R., Meissner, P.M., Schrader, K., Schwarz, K., 2019. Protein oxidation during temperature-induced amyloid aggregation of beta-lactoglobulin. *Food Chem.* 289, 223–231. <https://doi.org/10.1016/j.foodchem.2019.02.114>.

Keppler, J.K., Sönnichsen, F.D., Lorenzen, P.-C., Schwarz, K., 2014. Differences in heat stability and ligand binding among β-lactoglobulin genetic variants A, B and C using (1)H NMR and fluorescence quenching. *Biochim. Biophys. Acta* 1844 (6), 1083–1093. <https://doi.org/10.1016/j.bbapap.2014.02.007>.

Knowles, T.P.J., Mezzenga, R., 2016. Amyloid fibrils as building blocks for natural and artificial functional materials. *Adv. Mater. Weinheim.* 28 (31), 6546–6561. <https://doi.org/10.1002/adma.201505961>.

Krebs, M.R.H., Bromley, E.H.C., Donald, A.M., 2005. The binding of thioflavin-T to amyloid fibrils. *J. Struct. Biol.* 149 (1), 30–37. <https://doi.org/10.1016/j.jsb.2004.08.002>.

Krebs, M.R.H., Devlin, G.L., Donald, A.M., 2009. Amyloid fibril-like structure underlies the aggregate structure across the pH range for beta-lactoglobulin. *Biophys. J.* 96 (12), 5013–5019. <https://doi.org/10.1016/j.bpj.2009.03.028>.

Kroes-Nijboer, A., Venema, P., Bouman, J., van der Linden, E., 2011. Influence of protein hydrolysis on the growth kinetics of β-lg fibrils. *Langmuir* 27 (10), 5753–5761. <https://doi.org/10.1021/la104797u>.

Loveday, S.M., 2016. β-Lactoglobulin heat denaturation. *Int. Dairy J.* 52, 92–100. <https://doi.org/10.1016/j.idairyj.2015.08.001>.

Loveday, S.M., Anema, S.G., Singh, H., 2017. β-Lactoglobulin nanofibrils. *Int. Dairy J.* 67, 35–45. <https://doi.org/10.1016/j.idairyj.2016.09.011>.

Loveday, S.M., Su, J., Rao, M.A., Anema, S.G., Singh, H., 2012a. Whey protein nanofibrils. *J. Agric. Food Chem.* 60 (20), 5229–5236. <https://doi.org/10.1021/jf300367k>.

- Loveday, S.M., Wang, X.L., Rao, M.A., Anema, S.G., Creamer, L.K., Singh, H., 2010. Tuning the properties of β -lactoglobulin nanofibrils with pH, NaCl and CaCl₂. *Int. Dairy J.* 20 (9), 571–579. <https://doi.org/10.1016/j.idairyj.2010.02.014>.
- Loveday, S.M., Wang, X.L., Rao, M.A., Anema, S.G., Singh, H., 2011. Effect of pH, NaCl, CaCl₂ and temperature on self-assembly of β -lactoglobulin into nanofibrils. *J. Agric. Food Chem.* 59 (15), 8467–8474. <https://doi.org/10.1021/jf201870z>.
- Loveday, S.M., Wang, X.L., Rao, M.A., Anema, S.G., Singh, H., 2012b. β -Lactoglobulin nanofibrils. *Food Hydrocolloids* 27 (1), 242–249. <https://doi.org/10.1016/j.foodhyd.2011.07.001>.
- Macchioni, A., Ciancaleoni, G., Zuccaccia, C., Zuccaccia, D., 2008. Determining accurate molecular sizes in solution through NMR diffusion spectroscopy. *Chem. Soc. Rev.* 37 (3), 479–489. <https://doi.org/10.1039/b615067p>.
- Mishra, R., Sörgjerd, K., Nyström, S., Nordigården, A., Yu, Y.-C., Hammarström, P., 2007. Lysozyme amyloidogenesis is accelerated by specific nicking and fragmentation but decelerated by intact protein binding and conversion. *J. Mol. Biol.* 366 (3), 1029–1044. <https://doi.org/10.1016/j.jmb.2006.11.084>.
- Mohammadian, M., Madadlou, A., 2016. Cold-set hydrogels made of whey protein nanofibrils with different divalent cations. *Int. J. Biol. Macromol.* 89, 499–506. <https://doi.org/10.1016/j.ijbiomac.2016.05.009>.
- Ng, S.K., Nyam, K.L., Nehdi, I.A., Chong, G.H., Lai, O.M., Tan, C.P., 2016. Impact of stirring speed on β -lactoglobulin fibril formation. *Food Sci. Biotechnol.* 25 (S1), 15–21. <https://doi.org/10.1007/s10068-016-0093-8>.
- Nicolai, T., Durand, D., 2013. Controlled food protein aggregation for new functionality. *Curr. Opin. Colloid Interface Sci.* 18 (4), 249–256. <https://doi.org/10.1016/j.cocis.2013.03.001>.
- Pellarin, R., Caflich, A., 2006. Interpreting the aggregation kinetics of amyloid peptides. *J. Mol. Biol.* 360 (4), 882–892. <https://doi.org/10.1016/j.jmb.2006.05.033>.
- Peng, D., Yang, J., Li, J., Tang, C., Li, B., 2017. Foams stabilized by β -lactoglobulin amyloid fibrils. *J. Agric. Food Chem.* 65 (48), 10658–10665. <https://doi.org/10.1021/acs.jafc.7b03669>.
- Pitera, J.W., Falta, M., van Gunsteren, W.F., 2001. Dielectric properties of proteins from simulation. *Biophys. J.* 80 (6), 2546–2555. [https://doi.org/10.1016/S0006-3495\(01\)76226-1](https://doi.org/10.1016/S0006-3495(01)76226-1).
- Rahaman, T., Vasiljevic, T., Ramchandran, L., 2015. Conformational changes of β -lactoglobulin induced by shear, heat, and pH-Effects on antigenicity. *J. Dairy Sci.* 98 (7), 4255–4265. <https://doi.org/10.3168/jds.2014-9010>.
- Renard, D., Lefebvre, J., Griffin, M.C.A., Griffin, W.G., 1998. Effects of pH and salt environment on the association of β -lactoglobulin revealed by intrinsic fluorescence studies. *Int. J. Biol. Macromol.* 22 (1), 41–49. [https://doi.org/10.1016/S0141-8130\(97\)00086-X](https://doi.org/10.1016/S0141-8130(97)00086-X).
- Schleeger, M., vandenAkker, C.C., Deckert-Gaudig, T., Deckert, V., Velikov, K.P., Koenderink, G., et al., 2013. Amyloids. *Polymer* 54 (10), 2473–2488. <https://doi.org/10.1016/j.polymer.2013.02.029>.
- Serfert, Y., Lamprecht, C., Tan, C.-P., Keppler, J.K., Appel, E., Rossier-Miranda, F.J., et al., 2014. Characterisation and use of β -lactoglobulin fibrils for microencapsulation of lipophilic ingredients and oxidative stability thereof. *J. Food Eng.* 143, 53–61. <https://doi.org/10.1016/j.jfoodeng.2014.06.026>.
- van der Linden, E., Venema, P., 2007. Self-assembly and aggregation of proteins. *Curr. Opin. Colloid Interface Sci.* 12 (4–5), 158–165. <https://doi.org/10.1016/j.cocis.2007.07.010>.
- Wada, R., Fujita, Y., Kitabatake, N., 2006. Effects of heating at neutral and acid pH on the structure of beta-lactoglobulin A revealed by differential scanning calorimetry and circular dichroism spectroscopy. *Biochim. Biophys. Acta* 1760 (6), 841–847. <https://doi.org/10.1016/j.bbagen.2005.12.025>.
- Wang, W., Nema, S., Teagarden, D., 2010. Protein aggregation—pathways and influencing factors. *Int. J. Pharm.* 390 (2), 89–99. <https://doi.org/10.1016/j.ijpharm.2010.02.025>.
- Wit, J.N. de, Swinkels, G.A.M., 1980. A differential scanning calorimetric study of the thermal denaturation of bovine β -lactoglobulin Thermal behaviour at temperatures up to 100°C. *Biochim. Biophys. Acta Protein Struct.* 624 (1), 40–50. [https://doi.org/10.1016/0005-2795\(80\)90223-8](https://doi.org/10.1016/0005-2795(80)90223-8).
- Ye, X., Hedenqvist, M.S., Langton, M., Lendel, C., 2018. On the role of peptide hydrolysis for fibrillation kinetics and amyloid fibril morphology. *RSC Adv.* 8 (13), 6915–6924. <https://doi.org/10.1039/C7RA10981D>.
- Zhu, X., Guo, W., Jia, Y., Kang, F., 2015. Dielectric properties of raw milk as functions of protein content and temperature. *Food Bioprocess Technol.* 8 (3), 670–680. <https://doi.org/10.1007/s11947-014-1440-5>.